# A new design technique based on a suitable choice of rotor geometrical parameters to maximize torque and power factor in synchronous reluctance motors: Part I - Theory

Ivan Eduardo Chabu Viviane Cristine Silva Albert Foggia
José Roberto Cardoso Silvio I. Nabeta
LMAG/ EPUSP - Escola Politécnica da Universidade de São Paulo
Av. Prof. Luciano Gualberto, Trav. 3, 158 – 05508-900 São Paulo SP – Brazil
LEG - Laboratoire d'Electrotechnique de Grenoble – BP 46 – F-38402
St. Martin d'Hères Cedex – France

**Abstract** – The influence of rotor geometry of synchronous reluctance motors (SRMs) on the $x_d/x_q$ ratio, electromagnetic torque and iron losses is studied. Both air-gap length and rotor pole arc are taken into account as parameters. First, a new theoretical approach is developed which neglects saturation effects (Part I). In a companion paper (Part II), a complete finite-element analysis of a particular SRM is carried out, followed by a comparison with results obtained by tests performed in a prototype machine, which was constructed in order to validate the proposed methodology.

**Keywords:** Synchronous Reluctance Machines, synchronous machine design, reluctance motors.

## I. INTRODUCTION

Synchronous reluctance motors (SRMs) are widely used machines in industrial electric drives, with rated powers lying in the range of a few watts to some kilowatts.

Its main advantage is the association of an operation synchronized with power-supply frequency, with great reliability and robustness compared to, and to a certain extent even superior than, squirrel-cage induction motors, despite its lower efficiency and power factor (p.f.).

Typical applications are multi-motor drives, in which synchronism or rigorous speed-ratio shafts are the major requirements. In these cases, several SRMs, fed by a single frequency inverter, allow a wide range of operating variable speeds, keeping angular position synchronism among the motor shafts with greater advantage over the conventional systems, such as power selsyns or DC motors in master/slave configurations.

The use of SRMs greatly simplifies control systems. Moreover, they are simpler and their cost is lower than DC motors. The main applications include multi-motor conveyors, synchronized assembly lines, position control, large lifting equipment, textile machines, and so on.

PE-I169-EC-0-10-1997 A paper recommended and approved by the IEEE Electric Machinery Committee of the IEEE Power Engineering Society for publication in the IEEE Transactions on Energy Conversion. Manuscript submitted August 27, 1997; made available for printing October 7, 1997.

## II. GEOMETRICAL AND PHYSICAL FEATURES

While stator and polyphase windings are conventional, the SRM rotor is the main component for design purposes. It should present a variable magnetic reluctance along the air-gap, and several configurations are available that match this feature. Figure 1 illustrates some possible configurations, with distinct degrees of effectiveness and difficulty of construction.

The aim of these configurations is to obtain the largest possible difference between direct and quadrature-axis reluctances. Fig. 1a represents the most usual configuration, thanks to its simplicity of construction and relatively good performance. The others are more elaborate solutions to reach specific features like high synchronous pull-out torque or better p.f. at steady state.

In most of the available configurations, short-circuited bars are provided to enable asynchronous starting, as in conventional squirrel-cage motors, with the aim of producing high pull-in torque, and also to guarantee rotor synchronization even in the presence of loads with high inertia moments. Only in few cases is the cage discarded.

## III. POWER AND TORQUE CHARACTERISTICS

The analysis is based on the following hypotheses:

(i) the effect of stator ohmic losses on the torque developed by the motor will be neglected, since the value of stator ohmic resistance, $r_1$, in machines exceeding a few kilowatts is negligible compared to leakage and magnetizing reactances;
(ii) in a first step, the effects of iron saturation and iron losses will not be taken into account, with the analysis being conducted for the air-gap;
(iii) only the geometry presented in Fig. 1a will be considered, since it is the most common.

Thus, the phasor diagram allows the evaluation of both active and reactive power of a SRM at steady state, as depicted in Fig. 2.

The SRM can work in two different modes of operation, namely:

0885-8969/99/$10.00 © 1997 IEEE

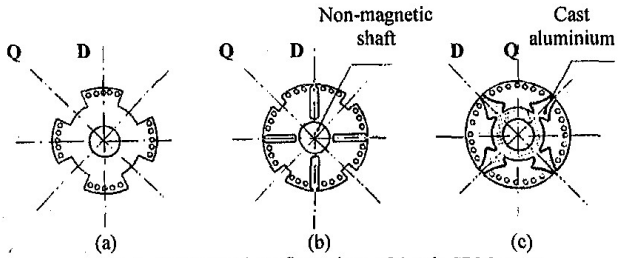


Fig. 1. Some usual configurations of 4-pole SRM rotors.

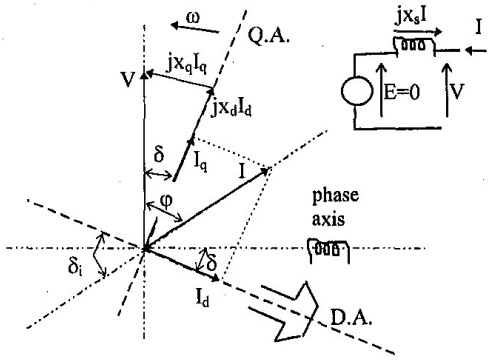


Fig. 2. Phasor diagram of the SRM at steady state (refer to the List of Symbols at the end of the paper).

(i) constant voltage supply, in which a constant voltage source is applied to the motor terminals. It represents the most usual operation mode, with the motor being fed by a voltage inverter;

(ii) constant current supply, less usual mode of operation, in which the motor is fed by a constant current source or current inverter. This mode of operation is mainly applied in SRMs working as position controllers, with the motor terminals subject to a direct current and phase commutation, behaving as a stepper motor.

From the phasor diagram in Fig. 2, the active and reactive power equations, per phase of the machine, for constant voltage operation can be derived, respectively, as (refer to the List of Symbols):

$$P_v = \frac{V^2}{2}\cdot\left(\frac{1}{x_q}-\frac{1}{x_d}\right)\cdot sin2\delta\,, \tag{1}$$

$$Q_v = V^2\cdot\left(\frac{sin^2\delta}{x_q}+\frac{cos^2\delta}{x_d}\right)\cdot sin2\delta\,, \tag{2}$$

and in the case of constant current operation, as:

$$P_i = \frac{I^2}{2}\cdot\left(x_d - x_q\right)\cdot sin2\delta_i\,, \tag{3}$$

$$Q_i = I^2\cdot\left(x_q\, sin^2\delta_i + x_d\, cos^2\delta_i\right). \tag{4}$$

Knowing the power equation and the synchronous angular speed, $\omega_s$, torque and p.f. as a function of load angle, $\delta$, can be promptly obtained, provided that reactances $x_d$ and $x_q$ are also known. Hence, let the spatial flux density distribution in the air-gap for both direct and quadrature axis (DA and QA) be imposed by spatially sinusoidal magnetomotive force (m.m.f.), as illustrated in Fig. 3.

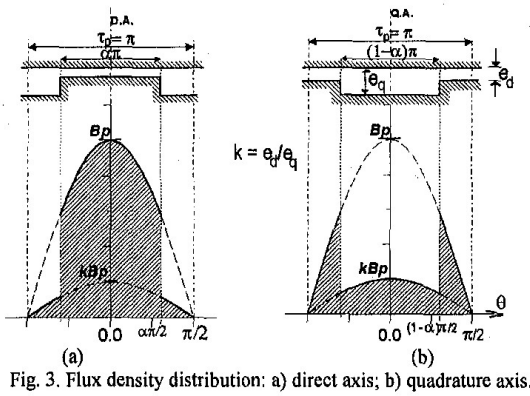


Fig. 3. Flux density distribution: a) direct axis; b) quadrature axis.

The flux per pole in the air-gap for both cases can be given by:

$$\phi_p = \frac{DL}{p}\cdot\int_0^{\frac{\pi}{2}} \boldsymbol{B}(\theta)\,d\theta\,, \tag{5}$$

The integration of (5) can be evaluated separately for the DA and QA and gives $\boldsymbol{B}_p f_d(\alpha,k)$ for the DA and $\boldsymbol{B}_p f_q(\alpha,k)$ for the QA, with the factors $f_d$ and $f_q$ given by:

$$f_d = k + (1-k)\cdot sin^{\alpha\pi}/_2\,, \tag{6}$$

$$f_q = 1 - (1-k)\cdot cos^{\alpha\pi}/_2\,, \tag{7}$$

and the parameter $k=e_d/e_q$, the ratio between the DA and QA air-gap lengths. Hence, (5) can be rewritten as:

$$\phi_p = D\cdot L\cdot B_p\cdot p^{-1}\cdot f(\alpha,k)\,, \tag{8}$$

with the factors $f=f_d$ in DA and $f=f_q$ in QA. Equation (8) can also be expressed in terms of the permeance of either the DA or the QA magnetic circuits, as follows:

$$\phi_p = F_p\cdot P(\alpha,k) = \left(B_p/\mu_0\right)\cdot e_d\cdot P(\alpha,k)\,.$$

Comparing this equation with (8), it yields:

$$P(\alpha,k) = \mu_0\cdot D\cdot L\cdot\left(p\cdot e_d\right)^{-1}\cdot f(\alpha,k)\,. \tag{9}$$

Now consider that for any pole of the machine the following equation holds:

$$N_p\cdot\phi_p = L_p\cdot I_{max} = N_p\cdot F_p\cdot P = L_p\cdot I_{rms}\cdot\sqrt{2}\,, \tag{10}$$

and also for a distributed and short-pitched winding with $m$ phases,

$$F_p = N_f \cdot k_w I_{rms} \cdot m \cdot \sqrt{2}/(\pi \cdot p). \quad (11)$$

Equations (10) and (11) yield:

$$P = \pi L_p \cdot 2p^2 / \left(N_{ph}^2 \cdot k_w^2 \cdot m\right),$$

which, compared to (9) and with the phase reactance given by $x_{ph} = \omega.2p.L_p$, yields:

$$x_{ph} = \left[\left(m\mu_0 \omega D L N_{ph}^2 k_w^2\right)/\left(\pi e_d k_g p^2\right)\right] \cdot f(\alpha, k)$$

and leads to the following expressions for the DA and QA synchronous reactances per phase:

$$x_d = A f_d \qquad x_q = A f_q \,, \quad (12)$$

with $A$ given by:

$$A = \left(m \cdot \mu_0 \cdot \omega \cdot D \cdot L \cdot N_{ph}^2 \cdot k_w^2\right)/\left(\pi \cdot e_d \cdot k_g \cdot p^2\right).$$

It should be noticed that reactances calculated by (12) are non-saturated values, related to the air-gap. However, these reactances can be corrected to take iron saturation into account by dividing those values by a suitable saturation factor, which assumes distinct values according to the axis considered, DA or QA, as will be developed later on.

An important indicative of the SRM performance is the ratio $x_d/x_q$, whose behavior as a function of rotor geometric parameters can be analyzed by observing Fig. 4, which presents the $x_d/x_q$ ratio as a function of the pole arc length, using $k$ as a parameter.

The torque characteristic is obtained from (1), (2) and (12) for constant-voltage and constant-current operation:

$$C_v = \frac{mV^2}{2\omega_s A} \cdot sin2\delta \cdot f_v \quad \text{and} \quad C_i = \frac{mI^2 A}{2\omega_s} \cdot sin2\delta_i \cdot f_i \,.$$

The quantities $f_v$ and $f_i$ depend on the rotor geometric parameters (see Fig. 5) and are called "torque factors". They are given by:

$$f_v = 1/f_q - 1/f_d \,, \quad f_i = f_d - f_q \,.$$

By rearranging (1), (2), (3) and (4) one can obtain the non-saturated p.f. for both constant-voltage and constant- current operation, as given respectively by:

$$\cos\varphi = \frac{\left(x_d/x_q - 1\right) \cdot sin2\delta}{2 \cdot \sqrt{\left\{\frac{\left[\left(x_d/x_q - 1\right)^2 \cdot sin^2 2\delta\right]}{4} + \left[\left(1 - x_d/x_q\right) \cdot sin^2\delta - 1\right]^2\right\}}} \,,$$

$$\cos\varphi_i = \frac{\left(1/x_d - 1/x_q\right) \cdot sin2\delta_i}{\sqrt{\left\{\left[\left(1/x_d - 1/x_q\right) \cdot \frac{sin\ 2\delta_i}{2}\right]^2 + \left(\frac{sin^2\delta_i}{x_q} + \frac{cos^2\delta_i}{x_d}\right)^2\right\}}}$$

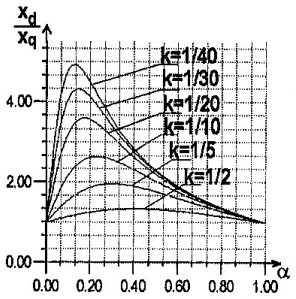


Fig. 4. $x_d/x_q$ ratio versus pole arc

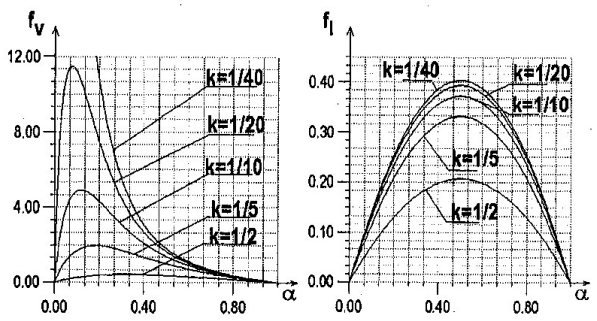


Fig. 5. Torque factors vs. pole arc

The variation of p.f. with rotor geometrical parameters can be seen in Fig. 6, with the ratio $x_d/x_q$ as a parameter and given in Fig. 4.

The p.f. represents the active and reactive powers associated only to the air-gap. In an actual machine, also the reactive power due to magnetic saturation is to be taken into account, as well as the active power related to iron losses, stator ohmic, mechanical and stray-load losses.

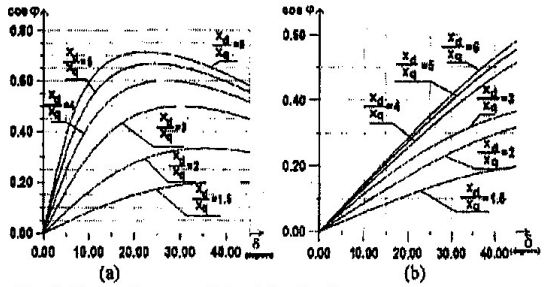


Fig. 6. Power factor vs. δ (see Fig. 2): a) constant-voltage and b) constant-current supply.

## IV. TOPICS ON THE SRM DESIGN

From the preceding section, it is possible to develop the SRM design procedure according to the kind of supply

(constant- voltage or constant current) to achieve a geometry which maximizes both torque and p.f.

In the case of constant voltage supply, Figs. 5b and 6a suggest that the lower the ratio $k=e_d/e_q$, between DA and QA air-gap lengths, the higher the torque and p.f. Therefore, the ratio $k=e_d/e_q$ is to be as short as possible, that is, with $e_d$ being as short as possible and $e_q$ as large as possible.

Mechanical constraints such as rotor peripheral speed and tolerance limit the DA air-gap, $e_d$, to the range 0.3 to 0.4 mm in machines with loads of a few kilowatts. In the case of the QA air-gap, there are less limitations. Usually, they refer to the rotor and shaft diameter, as well as the placement of cage bars.

Typical values of factor $k$ in motors for industrial purposes vary from 1/20 to 1/50.

It can be observed in Fig. 5b that the maximum torque occurs at reduced values of pole arc, $\alpha$, with the optimal value being less than 0.2 for the values of factor $k$ mentioned above. With the aid of Fig. 6a and Fig. 4 it can be noticed that the same analysis is valid for the p.f.. Nevertheless, a very short pole arc gives rise to some problems, e.g.:

(i) difficulty in placing the starting cage, which leads to a deficient design and hence difficults motor acceleration and reduces synchronization torque;

(ii) once dimensions and flux per pole have been defined (and hence stator slots volume and stator conductor cross section too), by reducing the pole arc, the stator current rises, due to an increase in reactive power consumption. Although the available active power also increases, one can observe a sharp increase in ohmic stator losses, since conductor cross section has been kept unchanged;

(iii) higher iron losses can arise with a reduction in pole arc, especially with $\alpha<0.4$.

In order to evaluate the increase in the iron losses at no-load, mainly in stator teeth, an analysis based on the r.m.s. flux density in the air-gap will be performed, which also affects the stator teeth. The r.m.s. flux density in the direct axis (see Fig. 3a) is written as:

$$B_{rms} = B_p \cdot \sqrt{\left\{\frac{k^2}{2} + \frac{(1-k^2)}{2} \cdot \left[\alpha + \frac{sin(1-\alpha)\cdot\pi}{\pi}\right]\right\}} \cdot$$

In the case of a cylindrical rotor one can assume $B_{rms_0} = B_{p_0}/\sqrt{2}$. Thus, for a salient-pole rotor with the same flux per pole as a smooth rotor, the iron losses in the teeth of the salient-pole motor can be evaluated by the ratio:

$$P_i/P_{i_0} = B_{rms}^2/B_{rms_0}^2 = \beta\,,$$

with

$$\beta = \left\{k^2 + (1-k^2)\cdot\left[\alpha + \frac{sin\pi\cdot(1-\alpha)}{\pi}\right]\right\}\cdot\left[k + (1-k)\cdot sin\frac{\alpha\pi}{2}\right]^{-2} \cdot \quad (13)$$

Furthermore, once the geometry is defined, the iron losses will increase in the stator teeth with an increase in load (increase in load angle $\delta$). For a given pole arc, say $\alpha=0.5$, the increase in iron losses with load can be evaluated by the factor (see Fig. 7b):

$$\gamma = \left[\frac{(1+k^2)}{2} + \frac{(1-k^2)}{\pi}cos2\delta\right]\cdot\left[k + \frac{(1-k)}{2}\sqrt{2}\,cos\delta\right]^{-2} \cdot \quad (14)$$

The ratio between the increase in iron losses for the stator teeth of the salient-pole machine and the one for the smooth-rotor machine is shown in Fig. 7a. Although the iron losses can be split into two components, one due to the stator teeth and other due to the stator yoke, even with the latter being constant, the former can be 4 to 6 times higher, for values of $k$ and $\alpha$ that maximize torque. This gives rise to global iron losses twice to 3 times as higher as the ones that arise in a machine with smooth rotor.

Hence, in the case of constant-voltage supply, it can be seen that using a reduced pole arc, although providing a increase in both SRM torque and power, does not guarantee a good design. Usually, depending on the problems mentioned above, values of pole arc are between 0.4 and 0.6.

In the case of constant-current supply, Fig. 5a and Fig. 6b show an optimal pole arc as 0.5.

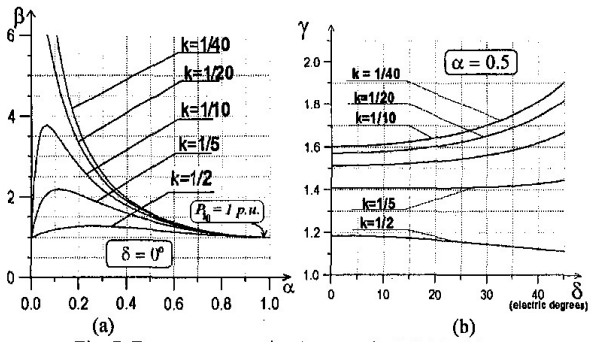


Fig. 7. Factors representing increase in SRM iron losses : (a) ratio between iron losses for salient-pole and smooth rotors as a function of rotor geometrical parameters at no-load ($\delta=0°$); (b) ratio between iron losses at load and at no-load for a given pole arc ($\alpha=0.5$).

## V. CALCULATION PROCEDURES OF A SRM

After selecting the best geometry according to the guidelines given so far, the methodology consists in solving two magnetic circuits: one for the DA and other for the QA. As a result, the synchronous reactances per phase, $x_d$, and $x_q$, can be determined, and then, with the aid of (1) and (2), active and reactive powers, as well as the torque, can be promptly obtained.

Stator ohmic and iron losses can also be calculated in the usual way, by assuming a smooth rotor. Then, the amount of iron losses associated with stator teeth is to be affected by the correction factors, $\beta$ and $\gamma$, given either by (13) and (14), respectively, or by Fig. 7. By adding these losses to the active power, one can evaluate both the efficiency and p.f. of the SRM.

Only the case of constant-voltage supply will be treated, since it is the most usual operation mode of the SRM.

Iron saturation effects on reactances $x_d$ and $x_q$ have not been discussed so far, but obviously this phenomenon plays a crucial role in the motor performance and should be taken into account.

Then, let us assume a constant-voltage operation with constant frequency. The flux per pole varies slightly when passing from the DA to the QA, due to stator leakage effects.

Despite this fact, the magnetic permeance falls sharply, which leads to an increase in flux densities and hence to an increase in saturation levels in the QA magnetic circuit. This also produces an increase in the $x_d/x_q$ ratio, thereby increasing the SRM torque and power.

In the case of a constant-current supply, the imposition of a m.m.f. with fixed amplitude dramatically reduces the flux per pole when passing from the DA to the QA. A decrease in the saturation level will then occur, thereby decreasing the $x_d/x_q$ ratio. The global effect over the SRM characteristics can be the opposite to those observed in the constant-voltage operation.

M.m.f. drops for the magnetic circuits are calculated in the usual way, with the aid of the magnetizing curve of the core material, thereby leading to saturated $x_d$ and $x_q$. To compute the air-gap, stator and rotor teeth m.m.f., it is necessary to know the shape factors of the flux density distributions in these regions, which are different for the DA and QA.

Through Fig. 3, shape factors can be computed as follows.

(i) For the DA air-gap and stator teeth:

$$k_{fds} = {}^{B_{av}}\!/_{B_p} = \left({}^{2}\!/_{\pi}\right)\cdot f_d(\alpha,k). \tag{14}$$

The integration for the rotor teeth is to be limited to the pole arc. Moreover, only the amount of the flux per pole which actually cross the rotor teeth should be taken into account. Therefore, the shape factor, corrected for the rotor teeth, becomes:

$$k_{fdr} = \left({}^{2}\!/_{\alpha\pi}\right)\cdot f_d(\alpha,k); \tag{15}$$

(ii) Repeating the procedure for the QA air-gap and stator teeth, one obtains:

$$k_{fqs} = {}^{B_{av}}\!/_{B_p} = \left({}^{2}\!/_{\pi}\right)\cdot f_q(\alpha,k), \tag{16}$$

and for the rotor teeth,

$$k_{fqr} = \left({}^{2}\!/_{\alpha\pi}\right)\cdot f_q(\alpha,k); \tag{17}$$

Fig. 8 presents the behavior of the shape factor as function on the rotor geometrical parameters.

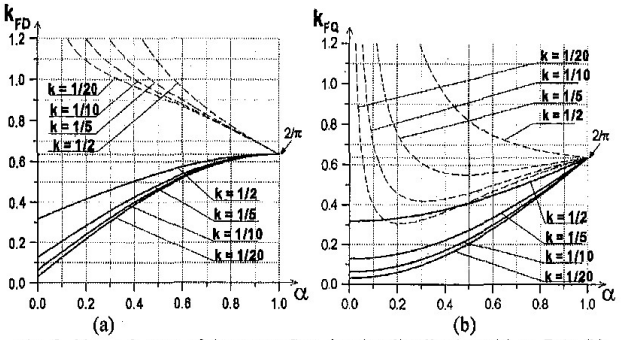


Fig. 8. Shape factors of the space flux density distribution: (a) on DA; (b) on QA. Subscripts s means air-gap (solid lines) and stator teeth; subscript r means rotor teeth (dotted lines).

It is worth mentioning that, in the case of a sinusoidal distribution of m.m.f., the flux density distribution will be only sinusoidal (or composed of patches of sinusoids) in linear media, e.g. in the air-gap. In saturated regions, such as stator and rotor teeth, the resulting distortion in the flux density curves yields distinct peak values that are required to impose a given flux, especially in presence of high saturation levels. This is usually the case in the rotor teeth located in the QA under constant-voltage operation.

Thus, in order to compute the magnetic field intensity required in stator and rotor teeth, the flux densities should be divided by some distortion factor. This factor is defined as the ratio between the peak value of a sinusoidal flux density curve and the peak value of the distorted curve, with both yielding the same value for an integration along a pole pitch, that is, the same flux per pole.

In [2], the distortion factor is taken as a constant value, $2/\sqrt{3} = 1/\cos 30°$, which is valid to flux densities varying from 1.4 to 1,8 T.

As the actual flux per pole is to be used in the calculation of magnetic circuits, the drop due to the stator leakage reactance, caused by the absorbed current, should be taken into account in the calculation. Since the absorbed current is determined after the evaluation of the magnetic circuit has been completed, this process becomes obviously iterative until a convergence for the current has been achieved.

This procedure requires a thorough evaluation of the leakage reactance, as well as the magnetic circuit, which is subject to high saturation levels, especially in the QA., so as to minimize errors.

On the other hand, the magnetic circuit can be evaluated through numerical methods such as the Finite Element Method, which enables a more precise determination of flux densities and hence the parameters of the machine. This is the subject of a companion paper: Part II - Finite Element Simulation versus Measurements.

## VI. CONCLUSIONS

New design procedures have been proposed so as to maximize both torque and power factor of SRMs, as well as to minimize iron losses. They are based on a theoretical

analysis of the influence of rotor geometrical parameters (e.g. air-gap length and pole arc) on those quantities. This influence (relating the electrical and mechanical quantities with geometrical parameters) is presented both in algebraic and graphical representation, thereby enabling the optimal choice of the relevant rotor geometrical parameters.

The validation and efficiency of the results obtained by the methodology are presented in a companion paper (Part II - Finite-element simulation versus measurements) in two different ways: first, they are compared with numerically simulated values provided by a 2D finite-element computer package. Finally, the two preceding methods are compared against measurements performed in a prototype machine.

## VII. LIST OF SYMBOLS

| | |
|---|---|
| $\alpha$, $\delta$, $\delta_i$ : | ratio pole arc/pole pitch and load angles (see Fig.2) |
| $e_d$, $e_q$ : | air-gaps in direct an quadrature axis, respectively |
| $k$, $k_g$ : | ratio of air-gaps ($e_d/e_q$) and Carter coefficient |
| $k_w$ : | winding factor (distribution and pitch) |
| $k_{fds}$, $k_{fqs}$: | shape factors for air-gap and stator teeth in DA and QA |
| $k_{fdr}$, $k_{fqr}$: | shape factors for rotor teeth in DA and QA |
| $L_p$, $P$ : | inductance per pole and permeance |
| $N_p$, $N_{ph}$: | number of turns per pole and per phase |
| $D$, $L$ : | stator internal diameter and length of the SRM |
| $m$, $p$ : | number of phases and pole pairs |
| $P_i$, $P_{i0}$ : | iron losses in the teeth of a salient-pole and smooth rotor machine |
| $\beta$ : | increase, due to the presence of salient poles, in the iron losses of an equivalent smooth-rotor machine |
| $\gamma$ : | increase, with load, in the no-load iron losses |
| $B_{av}$, $B_p$, $F_p$ : | average, peak spatial flux density and m.m.f. per pole |
| $B_{rms}$, $B_{rms0}$ : | r.m.s. value of DA flux density in the air-gap of salient-pole and smooth-rotor machine |
| $f_d$, $f_q$, $f_i$, $f_v$ : | geometric and torque factors |

## VIII. REFERENCES


[1] I.E. Chabu, J.R. Cardoso, "Projeto de motores elétricos pelo método dos elementos finitos: comparação analítica/numérica/experimental", Proceedings of II SIMEAR - International Seminar in Electrical Machines and Drives, 07-09th. May 1991, São Paulo, pp. 83-99 (in Portuguese).

[2] M.G. Say, "Alternating current machines", Longman Scientific & Technical, 5th edition

[3] P.J. Lawrenson, L.A. Agu, "Theory and Performance of Polyphase Reluctance machines", Proc. IEE, vol. III, n° 8, Aug. 1964.


## IX. BIOGRAPHIES

**Ivan Eduardo Chabu** was born in São Paulo, Brazil, in june 3, 1955. He obtained the B.Sc. and M.Sc. degrees in Electrical Engineering from *Escola Politécnica da Universidade de São Paulo* (EPUSP), Brazil. At the present he is pursuing the Ph.D. degree at EPUSP. He is currently working as a Lecturer at EPUSP and in the industry in design and construction of electrical machines. His main research interests are design of special electric machines and electromagnetic devices.

**Viviane Cristine Silva** was born in São Paulo, Brazil, in November 27, 1962. She obtained the BSc and MSc degrees in Electrical Engineering from *Escola Politécnica da Universidade de São Paulo* (EPUSP), Brazil. In 1994 she obtained the PhD degree in Electrical Engineering from *Institut National Polytechnique de Grenoble* (INPG), France. She is currently working as a Researcher at LMAG/EPUSP on Modelling and CAD in Electromagnetics. Her main research interests are 2D and 3D FE computation on electromagnetic fields

**Silvio Ikuyo Nabeta** was born in São Paulo, Brazil, in July 2, 1960. He obtained the BSc and MSc degrees in Electrical Engineering from *Escola Politécnica da Universidade de São* Paulo (EPUSP), Brazil. In 1994 he obtained the PhD degree in Electrical Engineering from *Institut National Polytechnique de Grenoble* (INPG), France. He is currently working as a Lecturer at EPUSP and his main research interests are 2D FE modelling of electrical machines and numerical techniques

**José Roberto Cardoso** was born in 1949. He obtained the B.Sc., M.Sc., Ph.D. and Liv.Doc. from *Escola Politécnica da Universidade de São Paulo* (EPUSP), Brazil, in 1974, 1979, 1985 and 1993, respectively. In 1975 he joined the Dept. of Electrical Engineering, EPUSP, as an Assistant Professor. He was promoted to Doctor Professor and Associate Professor in 1985 and 1993, respectively. In 1988 he founded the *LMAG-Laboratório de Eletromagnetismo Aplicado*. He was an invited researcher in *LEG-Laboratoire d'Electrotechnique de Grenoble*, France, in 1987/88. His current research interest includes electromagnetic field computation by FEM and electrical machines. He is currently the COMPUMAG'97 chairman.

**Albert Foggia** was born in Tunis (Tunisia) in April 12, 1942. He obtained his Engineer's and Doctor's degrees in 1964 and 1966 respectively from the *Institut National Polytechnique de Grenoble* (INPG). After graduation he went to Canada where he was assistant Professor at the Moucton University until 1969, and at *Ecole Polytechnique de Montreal* from 1969 to 1971. He came in 1971 to the *Ecole centrale de Lyon* where he was Professor until 1986. Since 1986 he has been Professor at INPG where he teachs electrical machine theory. His main research fields of interest deal with machine modelling, mechanical vibration of electrical machines and design of classical and non conventional machines.